Volume 11
Number 8
28 February 2020
Pages 1403-1534

Polymer Chemistry

rsc.li/polymers

ISSN 1759-9962

ROYAL SOCIETY OF CHEMISTRY

PAPER

Xiang-Kui Ren, Shuang Yang, Er-Qiang Chen *et al.*
Precise polyethylene derivatives bearing mesogenic side-chains: delicate self-assembly depending on graft density

Polymer Chemistry

ROYAL SOCIETY OF CHEMISTRY

PAPER

View Article Online
View Journal | View Issue

Cite this: *Polym. Chem.*, 2020, **11**, 1454

Precise polyethylene derivatives bearing mesogenic side-chains: delicate self-assembly depending on graft density†

Wen-Ying Chang,[a] Dong Shi,[a] Xu-Qiang Jiang,[a] Jia-Di Jiang,[a] Yang Zhao,[b] Xiang-Kui Ren, *[b] Shuang Yang *[a] and Er-Qiang Chen *[a]

Received 9th December 2019,
Accepted 6th January 2020

DOI: 10.1039/c9py01856e

rsc.li/polymers

To achieve desirable properties of side-chain polymers, elaborately manipulating the interplay between the polymer backbone and side-chains is vital, which can be done by adjusting the graft density of side-chains. Here, we report a series of polyethylene derivatives with the aromatic biphenyl side-chains precisely grafted on every 2nd, 7th and 15th carbon (**Pn**s, *n* = 2, 7, and 15) along the aliphatic backbone, the graft densities of which are nearly 4, 1, and 0.5 side-chains per nanometer, respectively. The self-assembly structures and phase transitions of **Pn**s were investigated using various techniques. We demonstrate that precisely adjusting the distance between two adjacent side-chains, *i.e.*, the side-chain spacing, can drastically alter the local coupling of the backbone and rod-like mesogenic side-chains, leading to different backbone conformations and anisotropic interactions. Compared to **P2** that is an ordinary side-chain liquid crystalline polymer (SCLCP) forming a crystal E phase, **P7** and **P15** exhibit a three-dimensionally (3D) ordered structure K_X and a two-dimensional (2D) rectangular columnar phase Col_R, respectively, which are unprecedented in SCLCPs. Moreover, the phase transition pathway can also be modified remarkably when the graft density is varied.

Introduction

Attaching side-groups/chains to the linear polymer backbone is a general strategy to develop advanced functional polymer materials.[1] For the same backbone, even slightly modifying the side-group structure can endow the polymers with very different mechanical properties and diverse responses to external stimuli.[2,3] Meanwhile, fundamental characteristics of the polymers can also be drastically changed. For example, atactic polypropylene, which just possesses a methyl side-group on every 2nd carbon along the backbone, has a plateau modulus nearly one fifth and a reptation tube diameter twice that of polyethylene (PE).[4] For side-chain polymers, the graft density is the key parameter determining the interactions between the side-chains and the linear backbone. With a fixed graft density, enlarging the side-group size can switch the chain from a coil to wormlike to a rod,[5,6] as the chain persistent length is increased systematically.[7,8] Increasing the graft density can result in a similar tendency, as exemplified by the polymers with a linear backbone and long side-chains.[9–11]

Practically, the graft density is usually adjusted by random copolymerization[12,13] or "grafting-to" methods.[11,14,15] As a result, although the average graft density can be estimated, the distance between every two adjacent side-groups/chains along the chain contour, *i.e.*, the side-chain spacing, is often not exactly controlled. To explicitly unveil the interplay between the side-chains and the backbone, precise side-chain polymers with a regular distribution of side-chains are highly desired. It has been demonstrated that precisely defined PE derivatives can provide a solid basis for the study on molecular dynamics and structures.[16–19] Wagener *et al.* have investigated systematically the precision-branched PE synthesized using the acyclic diene metathesis (ADMET) polymerization method.[20,21] For the samples with butyl as the pendant, when the spacing between two branches increases from 14 to 74 methylenes, the melting point increases from −33 to 104 °C, continuously approaching the melting point of ADMET synthesized linear PE at 134 °C.[22] Using the samples with different alkyls placed on every 21st carbon of the PE backbone, it has been found that the pendants larger than ethyl are excluded from the crystal, resulting in roughly the same melting temperature close to 20 °C.[23] Introducing functional groups to precision PE

[a]*Beijing National Laboratory for Molecular Sciences, Key Laboratory of Polymer Chemistry and Physics of Ministry of Education, Center for Soft Matter Science and Engineering, College of Chemistry, Peking University, Beijing, 100871, China. E-mail: eqchen@pku.edu.cn, yangshuang@iccas.ac.cn*

[b]*School of Chemical Engineering and Technology, Tianjin University, Tianjin, 300350, China. E-mail: renxiangkui@tju.edu.cn*

†Electronic supplementary information (ESI) available: Experimental details, molecular characterization, ^{1}H and ^{13}C NMR spectra of intermediates, monomers and polymers, X-ray data, molecular simulation results, reconstructed electron density map. See DOI: 10.1039/c9py01856e

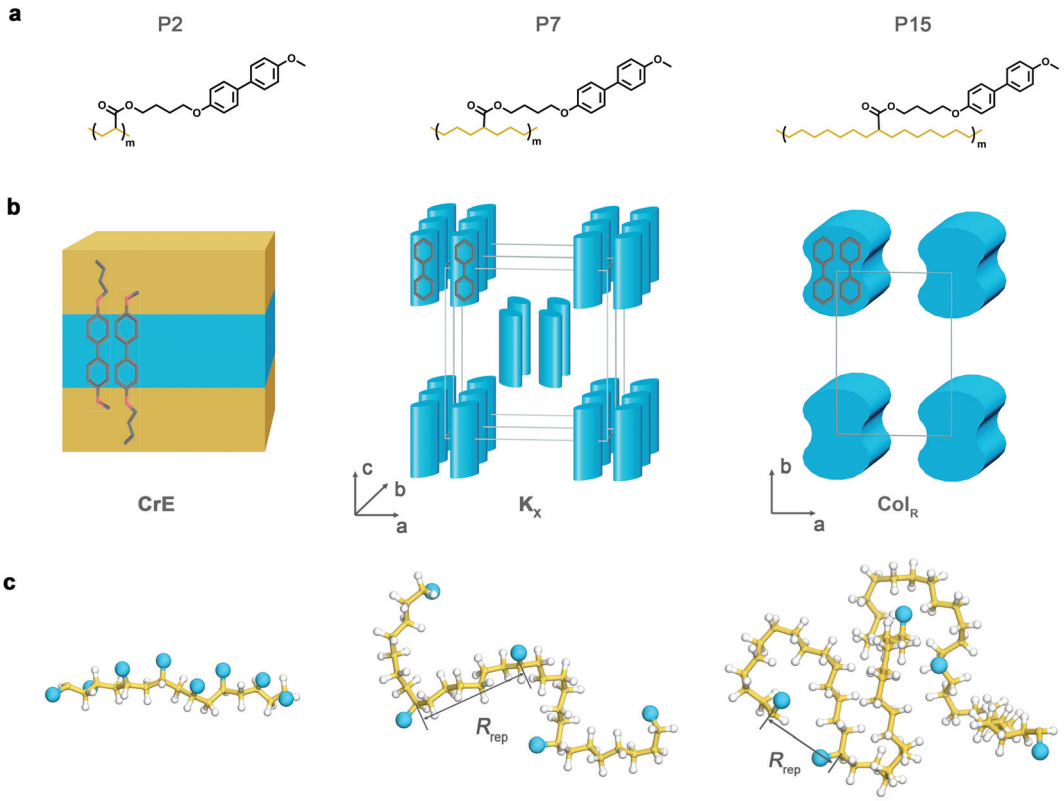

Scheme 1 (a) Chemical structures of P*n*s (n = 2, 7, and 15). (b) Schematic of CrE, K_X and Col_R for **P2**, **P7** and **P15**, respectively. The blue regions are occupied by the biphenyl groups. (c) Snapshots of chain models of P*n*s. To seek clarity, only the backbone is shown, and the side-chains are represented by blue spheroids. R_{rep} indicates the distance between two carbons on the backbone that connect the two adjacent side-chains.

also paves the way to advanced materials for energy and separation applications.[24]

It is very interesting to note that bearing a long branch of 21-carbon alkyl some precision PE samples may have better packing of molecules with different crystal morphologies.[25] It has been reported that with a large side-chain spacing the precise side-chain polyester can render sophisticated self-assembly with hierarchical structures.[26,27] These observations suggest that there exist complex interplays of main- and side-chains. In the present work, we accurately place rod-like mesogenic side-chains, which are aromatic rather than aliphatic, onto the PE backbone. We anticipate that the resultant side-chain liquid crystalline polymer (SCLCP) can render "local coupling" between the backbone and side-chains more sensitive to the variation of the side-chain spacing, considering the tendency of nano-segregation between aromatic and aliphatic components and the anisotropic interactions of mesogens. In consequence, it would be possible to reveal the coupling mechanism at different graft densities in a more quantitative way, namely, how the side-chains affect the backbone conformation and how the main-chain regulates simultaneously the self-assembly of side-chains. It is well known that insertion of a reasonably long "flexible spacer" between the backbone and mesogen is apt to promote the liquid crystal (LC) ordering in SCLCPs due to the dynamic decoupling of the backbone and side-chains.[28–30] However, the graft density effect has not been well addressed so far.[31–33]

The precise SCLCPs we study here possess biphenyl side-chains on every 2nd, 7th and 15th carbon of the PE backbone, respectively (**P*n***, n = 2, 7, and 15, Scheme 1a). **P2** was obtained using controlled radical polymerization. **P7** and **P15** were prepared using ADMET polymerization followed by hydrogenation.[23] We will show that, compared with **P2** forming a crystal E (CrE) phase, **P7** exhibits a three-dimensionally (3D) ordered structure (K_X) and **P15** a two-dimensional (2D) rectangular columnar phase (Col_R), which are unusual in SCLCPs (Scheme 1b). It is found that the mesogenic side-chains exert a great influence on the backbone conformation (Scheme 1c). The **P2** backbone with the highest graft density is largely extended. On the length scale of the repeating unit, **P7** is quite stiff and **P15** is quite flexible. The compromise due to the coupling of the backbone and biphenyls results in dramatically changed molecular packings and phase transition behaviors.

Results and discussion

Synthesis and polymerization

As a typical SCLCP, **P2** was obtained from the corresponding acrylate monomer by reversible addition–fragmentation chain

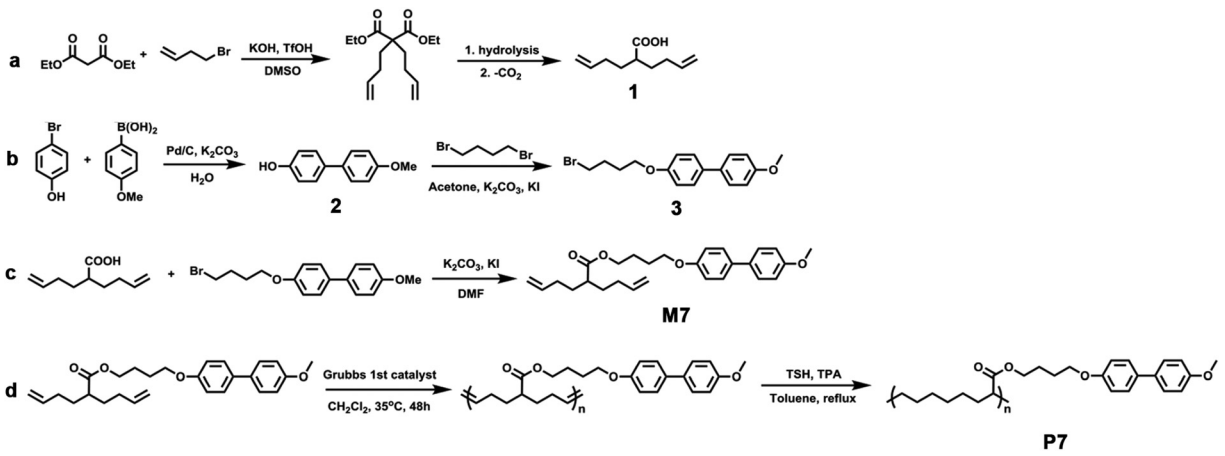

Fig. 1 Synthetic routes of **M7** and **P7**.

transfer (RAFT) polymerization. To get **P7** and **P15**, the synthesis was more complex, as the α,ω-diene monomers were needed to be prepared first. Using **P7** as an example, the synthetic route is illustrated in Fig. 1. In brief, 2-(3-buten-1-yl)-5-hexenoic acid (**1**) was synthesized using diethyl malonate and 4-bromo-1-butene as raw materials (Fig. 1a). 4-(4-Bromobutoxy)-4′-methoxy-1,1′-biphenyl (**3**) was obtained by two steps of substitution reaction (Fig. 1b). As shown in Fig. 1c, nucleophilic substitution of **1** and **3** led to the monomer **M7**. At 35 °C, **M7** was polymerized by the ADMET method using the Grubbs 1st catalyst for 48 h. Successive nitrogen purge was used to remove the by-product ethylene. Afterwards, hydrogenation resulted in the polymer **P7**. **M15** and **P15** were synthesized in the same way.

Detailed synthesis and molecular characterization are described in the ESI.† All the intermediates and monomers were well characterized using various techniques with the satisfactory analysis data. Owing to the condensation polymerization mechanism of ADMET, molecular weight (MW) distributions of the crude polymers of **P7** and **P15** were broad; thus, MW fractionation was carried out. As shown in Table 1, the fractionated samples possessed a number-averaged MW (M_n) of ~1.9 × 10^4 g mol^{-1} and a polydispersity index (PDI) of ~1.4 measured by gel permeation chromatography (GPC) calibrated using polystyrene standards. It was hard to get **P2** with a high MW (see Table 1, M_n of 4.5 × 10^3 g mol^{-1}), probably due to the poor solubility of the polymer in the solvent during polymerization. Nevertheless, we found that the obtained samples of **P2** could show the phase structure affected little by the MW.

Table 1 also lists the weight fractions of biphenyl mesogens in **Pn**s. Assuming that the ordered packed biphenyl groups possess a density of 1.25 g cm^{-3} (such as in the CrE phase), the biphenyl volume fractions were estimated based on the measured density, which are decreased from 64% to 34% with n increasing from 2 to 15. In this case, the change of physical properties of **Pn**s could be anticipated.

Table 1 Molecular characteristics of **Pn**s

Sample	M_n[a] (kg mol^{-1})	PDI[a]	Density[b] (g cm^{-3})	W_{biph}[c] (%)	f_{biph}[c] (%)
P2	4.5	1.12	1.18	61	64
P7	18.5	1.41	1.14	50	46
P15	19.7	1.37	1.08	39	34

[a] Number average molecular weight (M_n) and polydispersity index (PDI) were measured by GPC calibrated with polystyrene standards. [b] Experimental density measured using a floating method. [c] W_{biph} and f_{biph} are the weight and volume fractions of biphenyl mesogens, respectively.

Phase identification

We identified the phase structures of **Pn**s using X-ray diffraction (XRD). Well-developed ordered structures could be obtained by annealing **Pn**s at temperatures slightly below their isotropic temperatures (T_is). In the one-dimensional (1D) XRD profile (Fig. 2), **P2** presents low angle diffractions with a q-ratio

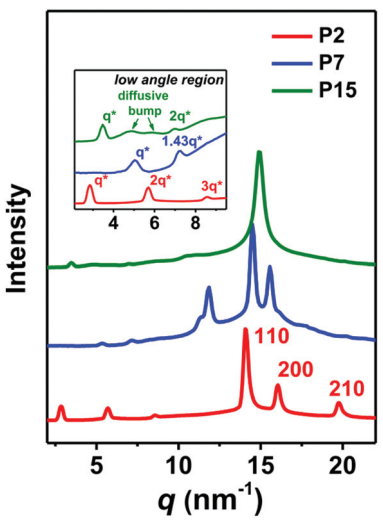

Fig. 2 1D XRD profiles of **Pn**s after annealing at temperatures slightly below their T_is recorded at room temperature.

($q = 4\pi \sin\theta/\lambda$, with 2θ being the scattering angle and λ being the wavelength) of 1 : 2 : 3, manifesting a smectic-like layer structure with a period of 2.22 nm. On the other hand, the three sharp diffractions in the high angle region can be indexed as (110), (200) and (210), respectively. Thus, an orthorhombic lattice of CrE with a = 0.78 nm, b = 0.54 nm and c = 2.22 nm can be determined (Table S1†), which is similar to that reported in the literature.[34,35]

While the CrE phase can be readily resolved for **P2**, the 1D XRD results of **P7** and **P15** indicate that their structures are more complex than the conventional LC phases (Fig. 2). **P7** renders quite a few diffractions in both low and high angle regions, evidencing a highly ordered structure of molecular packing. For **P15**, a strong single diffraction is observed at 0.43 nm in the high angle region, reminiscent of the hexagonal packing of mesogens in the hexatic or crystal B phase. On the other hand, in the low angle region, scattering bumps can be well recognized in addition to the first diffraction at 1.81 nm. This outcome suggests that there exists a special self-assembly other than the layer structure on the nanometer scale.

To determine the LC structures of **P7** and **P15**, which we denote as K_X and Col_R, respectively, 2D XRD was employed. The orientated samples were prepared by mechanical shearing when the temperature became just slightly below T_i upon cooling. The 2D XRD patterns of the uniaxially oriented samples are shown in Fig. 3, with the shear direction assumed as the meridian. For K_X in **P7**, according to the diffraction geometry, the spots 1 on the meridian, 2, 3 and 4 in the quadrants, and 5 on the equator in Fig. 3a are assigned to be (002), (101), (112), (301) and (310), respectively. As a result, all the diffractions detected for **P7** can be well indexed using an orthorhombic lattice with a = 1.62 nm, b = 0.80 nm and c = 1.74 nm (Table S2†).

For Col_R in **P15**, we paid attention to the scatterings in the low angle region. The spots 1′ on the meridian (shear direction) and 2′ and 3′ in Fig. 3b can be indexed as (01), (10) and (11), respectively. Thus a 2D rectangular unit cell of Col_R with a = 1.27 nm and b = 1.81 nm can be determined. Compared with the sharp diffraction (01), the spot of (10) on the equator is diffusive, indicating that the correlation length along the a-axis is relatively short in Col_R. On the other hand, the strong diffraction in the high angle region at 0.43 nm concentrated on the equator is attributed to the packing of the mesogens of biphenyl that are parallel to the shear direction.

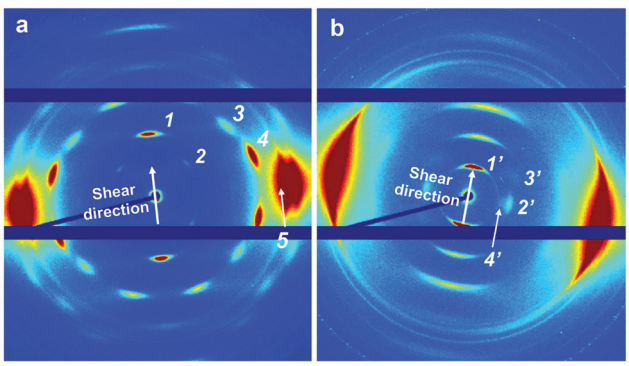

Fig. 3 2D XRD patterns of oriented (a) **P7** and (b) **P15** after annealing recorded at room temperature.

Molecular packing scheme

The aforementioned results show clearly that the phase structures of **P*n***s change significantly when the side-chain spacing is precisely tuned. The molecular packing schemes of **P*n***s were further investigated, with the aid of reconstruction of a relative electron density map (EDM) and molecular simulation (see ESI†).

P2 is actually an ordinary SCLCP, similar to other SCLCPs synthesized from vinyl monomers.[36] The EDM of the layer structure of **P2** was calculated based on the four low angle diffractions (Fig. S1†). Within the layer period, two electron density maxima and two minima can be clearly seen from the 1D electron density variation along the layer normal. For **P2**, the extended side-chain length measured from the carbon on the backbone to the carbon on the methoxy end group is 1.88 nm, 0.34 nm smaller than the layer period of 2.22 nm determined experimentally (Fig. S2a†). As a result, a monolayer structure, which is similar to the interdigitated smectic A (SmA_d),[37] can be inferred.

We presume that in the CrE of **P2**, the biphenyl groups emanating from the adjacent main-chain layers can interdigitate and interact together, forming a biphenyl layer with the highest electron density (Fig. S2b†). On the other hand, the spacers and the methoxy groups are arranged in the space between the biphenyl and main-chain layers, corresponding to the minimum of the electron density. In CrE, the biphenyl mesogens should exhibit a herringbone array.[34,35] The **P2** main-chains are squeezed in a very thin space with a thickness of ~0.5 nm in the smectic-like structure. The atactic structure of the **P2** main-chain and the chain ends can introduce significant defects in the molecular packing, and thus may prevent the propagation of the crystalline order of biphenyl along the layer normal.[38]

Of particular interest is that **P7** and **P15** abandon the smectic structure that prevails in SCLCPs. As schematically drawn in Scheme 1b, **P7** has the biphenyl mesogens registered in the orthorhombic lattice of K_X, and the mesogens of **P15** form columns embedded in the aliphatic mixture.

According to the orthorhombic lattice of **P7** and the measured density, it is found that the unit cell of K_X contains 4 repeating units and thus 4 biphenyls. This result is supported by the 3D EDM of **P7** calculated based on the 7 indexed diffractions (see ESI, Fig. 4a and S3†). In the EDM in Fig. 4a, the vertical bar-like and horizontal meniscus-like domains suggest the approximate locations of biphenyl and carbonyl groups, respectively, which have electron densities higher than the aliphatic components. The EDM indicates that the biphenyls are parallel to the c-axis (the shear direction in Fig. 3a), in agreement with the strong high angle diffractions on the equator. Interestingly, we find that in the lattice two adjacent

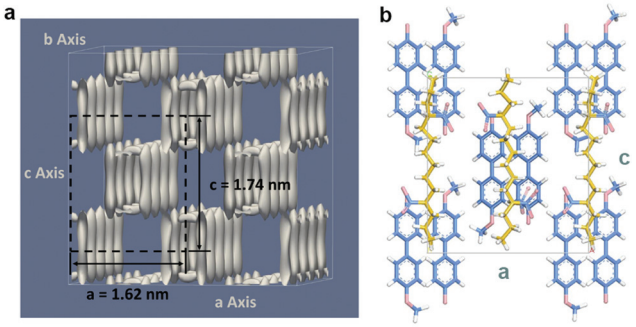

Fig. 4 (a) Reconstructed 3D EDM of K_X of **P7**. The display box size is 3.2 nm × 3.2 nm × 3.2 nm. The vertical bar-like and horizontal meniscus-like domains correspond to the approximate locations of biphenyl and carbonyl groups, respectively. (b) Possible molecular packings of **P7** in K_X viewed along the *b*-axis.

biphenyl groups on the *ac* plane form a "pair". Furthermore, the two "pairs" in the orthorhombic lattice are located at (0, 0, 0) and (1/2, 1/2, 1/2), respectively. Namely, along the *b*-axis, two neighboring "pairs" are separated with a distance of 0.8 nm. In this case, the π–π interaction of biphenyls is not maximized in K_X, and the methylene units have to fill the space between the biphenyl "pairs".

To reveal how the methylene units pack in K_X of **P7**, we performed polarized FT-IR experiments on the sheared **P7** after thermal annealing. In the CH_2 bending region (1440–1485 cm^{-1}), the absorption bands at ~1475 and ~1468 cm^{-1} correspond to the *trans*- and *gauche*-dominated conformation, respectively, the vibration directions of which are perpendicular to the axis of the methylene segment (Fig. S4†). Fig. 5a of oriented **P7** shows that the 1475 cm^{-1} band at a polarizing angle of 0° (*i.e.*, the polarizer is parallel to the shear direction) is much weaker than that at 90°, giving a dichroic ratio $A_{\parallel}/A_{\perp}$ of 0.08. Thus, the *trans*-dominated methylene segments are largely distributed parallel to the *c*-axis of K_X.

Note that the extended length of two repeating units of **P7** is 1.80 nm, slightly larger than the *c* of K_X (1.74 nm). With this in mind, we gave the most possible conformation and chain packing of **P7** in K_X by use of molecular simulation (Fig. 4b). The backbone, which is extended, intercalates in the vacancy between two parallel "pairs" of biphenyls. After going through the "pairs", the main-chain can have the carbonyl group to further connect the biphenyl group through the spacer. The simulated diffraction profile of the molecular model agreed with the experimental XRD result (Table S2 and Fig. S5†). The K_X of **P7** can be viewed as a kind of soft crystal. We note that, without the control of tacticity, the carbonyls can point to either the left or right, and the spacers may have some disordered conformations. Therefore, some intrinsic defects and local disorders exist in K_X.

P15 presents sharp low angle diffractions on the meridian with the first order one at 1.81 nm. One may presume that **P15** still presents the smectic-like layer structure. However, the volume fraction of biphenyls is estimated to be ~34% (Table 1). If the common layered structure were assumed, the biphenyl layer thickness would be ~0.61 nm (= 0.34 × 1.81 nm). As mentioned above, the strong diffraction concentrated on the equator at 0.43 nm indicates that the mesogens are perpendicular to the layer surface. Therefore, the thickness of 0.61 nm is too small compared to the length of biphenyl. Consequently, **P15** will have some unique nano-segregation morphology different from the structure such as hexatic B or crystal B.

Using the three diffractions/scatterings shown in the low angle region, *i.e.*, 1′, 2′ and 3′ indicated in Fig. 3b, we calculated the 2D EDM of **P15**. The scatterings 2′ and 3′ are weak; however, they constantly appeared when the ordered molecular packing of **P15** was well developed, indicating that they reflect the intrinsic nano-segregation between the aromatic and aliphatic components in **P15**.[39] The EDM in Fig. 6a shows that on the nanometer scale **P15** has the columns (the red area) arranged in a 2D rectangular lattice with the *p2mm* symmetry. Within the columns that have higher electron density, the biphenyls will pack parallel to each other (Scheme 1b). Compared to the ordinary smectic structures of SCLCPs, we think that in **P15** the columns are resulted from slicing the mesogen layers, suggesting a frustrated molecular packing.

Polarized FT-IR experiment on the oriented **P15** shows that for the 1476 and 1466 cm^{-1} bands the dichroic ratios of $A_{/\!/}/A_{\perp}$

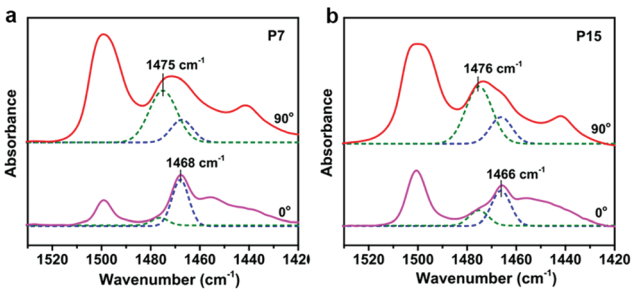

Fig. 5 Polarized FT-IR spectra of oriented (a) **P7** and (b) **P15** with 0° (parallel) and 90° (perpendicular) rotating polarized angles with respect to the shear direction. The dashed curves correspond to *trans*- (1475 or 1476 cm^{-1}) and *gauche*- (1466 or 1468 cm^{-1}) dominated conformations.

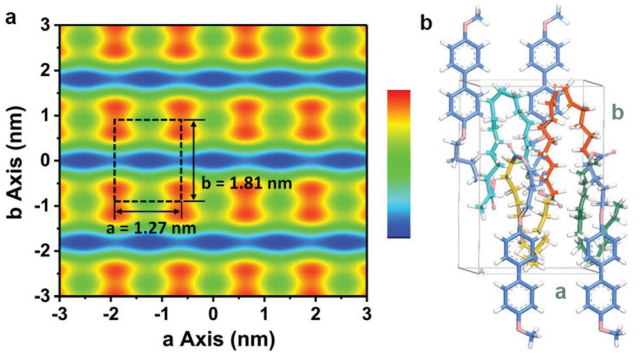

Fig. 6 (a) Reconstructed 2D EDM result and (b) possible molecular packings of **P15** in Col_R. In (b), one **P15** chain containing 4 repeating units is shown; the biphenyl groups are parallel to the *b*-axis.

are 0.18 and 1.12, respectively (Fig. 5b). The outcome suggests that in Col_R the *trans*-dominated methylene segments tend to be parallel with the *b*-axis and thus the biphenyls. However, the *gauche*-dominated ones have no obvious preferential orientation. Accordingly, we built a molecular model to show the possible way of how the space in Col_R can be filled (Fig. 6b). Between the mesogen columns, the methylene segments that are long enough can form folds. The folded parts contain more *gauche* conformation, and the parts that are more parallel to biphenyl can be *trans*-dominant. Note that there is a weak and diffusive scattering at 1.63 nm on the equator (indexed as 4′ in Fig. 3b), evidencing an additional density fluctuation. Assuming that this fluctuation is perpendicular to not only the *b*-axis but also the *a*-axis, the columns in Col_R would be undulated (Table S3 and Fig. S6†). With a volume fraction of ~66%, the aliphatic component might squeeze the columns in a sort of periodical manner.

Chain conformation dependence

We consider that the different molecular packings of **Pn**s are closely associated with the chain conformation that depends on the side-chain spacing. Using molecular simulation, we created the single chains of **Pn**s in the melt state, each of them containing 30 repeating units linked together in a head-to-tail fashion (Fig. S7†). Snapshots in Scheme 1c highlight the simulated backbone conformations of **Pn**s.

Assuming an all-*trans* polyethylene backbone, the graft density of **P2** is ~4 nm^{-1}. Such a compact arrangement of side-chains can induce strong steric hindrance, making the main-chain stretched. In **P7** and **P15**, the graft density is reduced to ~1 and ~0.5 nm^{-1}, respectively. Both the **P7** and **P15** chains are random coils as a whole; however, at the repeating unit level they have different conformations (Fig. S7†). We measured the distance between two carbons on the backbone that connect the two adjacent side-chains (R_{rep}, indicated in Scheme 1c). The distributions of R_{rep}s of **P7** and **P15** are shown in Fig. 7 and the calculated number average values ($<R_{rep}>$s) are listed in Table S4.† Interestingly, **P7** has a pretty narrow distribution of R_{rep}, and its $<R_{rep}>$ is ~0.76 nm, close to the monomer length with all-*trans* conformation (0.90 nm). Thus, the **P7** repeating unit is stiff, indicating that the side-chains still hamper the rotation of C–C bonds on the backbone to a large extent. For **P15**, which has an extended monomer length of 1.87 nm, the $<R_{rep}>$ is just ~1.15 nm, and the values of R_{rep} exhibit a broad distribution. Therefore, the backbone in **P15** is flexible and the methylene segments between the two adjacent side-chains on the backbone can present frequently fold-like shapes.

The conformation differences help us to understand the molecular packing behaviours of **Pn**s. With the extended backbone, the **P2** chain may be ribbon-like as a whole in CrE.[30] The main-chains of **P2** can lie in the narrow space between two adjacent biphenyl layers, adapting to the strong confinement imposed from both sides. However, such confinement will be largely released in **P15**, which is due to the rather flexible backbone with a larger conformational entropy. To maximize the anisotropic interactions, mesogens are always apt to pack into a layer structure with the lateral dimensions as large as possible. However, the entropy elastic force from the **P15** backbone will resist such mesogen layers, since they will cause compression. The balance of enthalpy and entropy leads the mesogen layer to be sliced into columns and thus to the structure of Col_R. The 3D ordered K_X of **P7** is a bit astonishing, considering that the chain tacticity is uncontrolled. The precisely placed side-chains offer **P7** with a kind of regularity in the chemical structure. Moreover, the pretty stiff repeating unit, which has a length close to that of biphenyl, should be of vital importance. While the π–π interaction is not sufficiently developed, the energy can be reduced when the backbone adopts nearly all-*trans* conformation.

Phase transition behaviours

Precise variation of the side-chain spacing also influences the phase transition process. Differential scanning calorimetry (DSC) results show that **P2** and **P15** exhibit enantiotropic transition with T_is at 78 and 143 °C, respectively (Fig. 8). For **P2** and **P15**, the onsets of transitions observed during cooling are rather close to that found during heating, which shows the feature of LC transition that is close to equilibrium. Subsequent thermal annealing hardly shifts their T_is. Differently, **P7** presents a monotropic transition. As shown in Fig. 8, a small but sharp peak at 74 °C appears firstly during

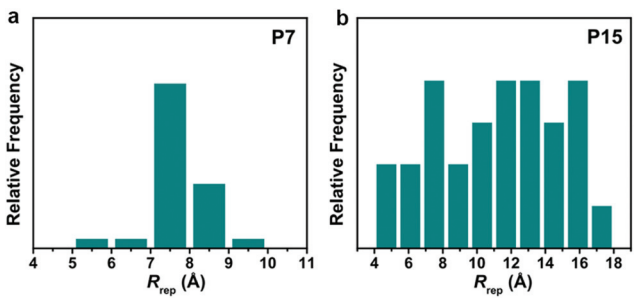

Fig. 7 Distribution of R_{rep}s of (a) **P7** and (b) **P15** measured from molecular simulation of single chains in the melt state (at 473 K).

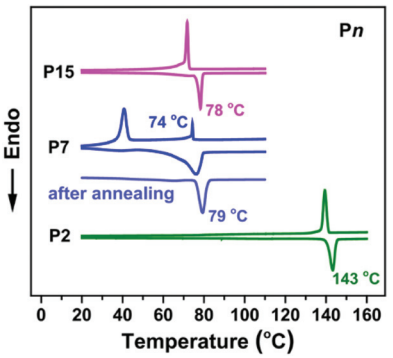

Fig. 8 DSC cooling and subsequent heating traces of **Pn**s and heating trace of the annealed **P7** recorded at a rate of 5 °C min^{-1}.

cooling. Thermal XRD and polarized light microscopy (PLM) experiments reveal that this transition is associated with a nematic (N) phase (Fig. 9a and S8a†). Interestingly, shearing **P7** in the N phase could change the schlieren texture to the banded one (Fig. 9b), which is rarely observed in SCLCPs. The metastable N phase would transfer to the stable K_X phase. Relatively fast cooling at 5 °C min^{-1} could result in an imperfect K_X, suggested by the broad endotherm observed during heating right after the cooling process. However, slow cooling or thermal annealing of **P7** can lead to a sharp endotherm peak appearing at 79 °C (Fig. 8), which corresponds to the transition from the stable K_X to the isotropic state.

We also estimated the entropy changes of isotropization (ΔS_is) from DSC heating results of the annealed **P*n*s**, which are 27.0, 37.5 and 83.6 J mol^{-1} K^{-1} for **P2**, **P7** and **P15**, respectively. The variation of ΔS_i of **P*n*s** reflects that the entropy of the isotropic melt arises when enlarging the side-chain spacing, coinciding with the increase of backbone flexibility. Moreover, the ΔS_i should also associate with the mobility of mesogens in the melt. In **P2**, the mesogens tethered densely along the backbone through the four methylene linkage are rather close to each other. In this case, the side-chain motion is limited and a sort of "preorder" may exist that facilitates the phase transition. By contrast, with the lowest graft density, **P15** has a weak local coupling of side-chains and the backbone, and the separation between the aromatic and aliphatic components promotes the direct formation of Col_R during cooling. For **P7**, worth noting is that the lengths of biphenyl and $\langle R_{rep} \rangle$ are comparable. When entering the LC state, the relatively weakened effect of local coupling could lead the prolate backbones to tend to be parallel to the biphenyls as predicted by theory,[40] forming a type-III nematic (N_{III}) with a low energy barrier.[30] We presume that the N_{III} phase may be the reason for the shear-induced banded texture. After the formation of N_{III}, the delicate adjustment of the mesogen and backbone position, which is kinetically slow, will result in the 3D ordered K_X phase. Note that in the K_X of **P7** the backbones intercalate the "pairs" of biphenyls; namely, the backbones and biphenyls share the same orientation. Therefore, during the N-to-K_X transition, the main feature of N_{III} has been retained.

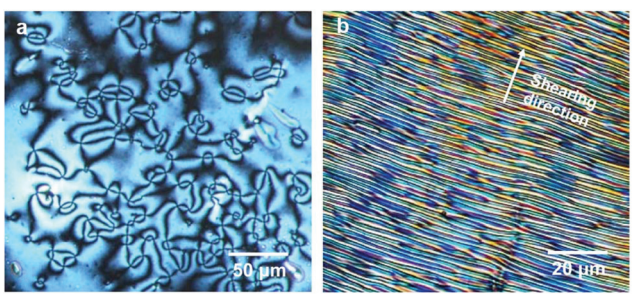

Fig. 9 PLM images of (a) the schlieren texture of **P7** at 70 °C and (b) banded texture obtained by shearing **P7** in the N phase.

Conclusion

In summary, we have synthesized three **P*n*s** (n = 2, 7 and 15) with the biphenyl-containing side-chains precisely placed on every 2nd, 7th and 15th carbon on the polyethylene backbone, respectively. To illustrate the effect of side-chain spacing or graft density on the side-chain/backbone interplay and the molecular ordering, the three samples were carefully examined and compared. The **P2** chains are quite extended because of the highest graft density, and can pack into the CrE phase with a smectic-like layer structure. Having the largest side-chain spacing, **P15** exhibits the 2D ordered columnar phase Col_R with a frustrated molecular packing. This is due to that the entropy elastic force of the backbone opposes the formation of a continuous mesogen layer. While that of **P2** and **P15** is enantiotropic, the phase transition of **P7** is monotropic with the metastable N phase observed during cooling. The **P7** backbone is stiff at the repeating unit level. The backbone can become extended and fit in the stable K_X phase with a 3D ordering. This work discloses that the side-chain spacing, one of the key structure factors that can be regulated by chemistry, can bring about a significant influence on the self-assembly behaviours and physical properties of side-chain polymers. We anticipate that future studies on the side-chain spacing effect can greatly facilitate the materials designs of polymers bearing pendants, promoting the molecular engineering of advanced materials.

Conflicts of interest

There are no conflicts to declare.

Acknowledgements

The work was supported by the National Natural Science Foundation of China (Grants 21634001 and 21875157) and the National Key R&D Program of China (2018YFB0703703). We are grateful to Prof. Zi-Chen Li and Dr Jian Zhang for the help and discussions on synthesis.

References

1 P. C. Hiemenz and T. P. Lodge, *Polymer Chemistry: Second Edition*, CRC, United States, 2007.
2 E. Blasco, M. B. Sims, A. S. Goldmann, B. S. Sumerlin and C. Barner-Kowollik, *Macromolecules*, 2017, **50**, 5215–5252.
3 M. A. Gauthier, M. I. Gibson and H. A. Klok, *Angew. Chem., Int. Ed.*, 2009, **48**, 48–58.
4 L. J. Fetters, D. J. Lohse, D. Richter, T. A. Witten and A. Zirkel, *Macromolecules*, 1994, **27**, 4639–4647.
5 B. M. Rosen, C. J. Wilson, D. A. Wilson, M. Peterca, M. R. Imam and V. Percec, *Chem. Rev.*, 2009, **109**, 6275–6540.
6 B. Zhang, R. Wepf, K. Fischer, M. Schmidt, S. Besse, P. Lindner, B. T. King, R. Sigel, P. Schurtenberger,

Y. Talmon, Y. Ding, M. Kroger, A. Halperin and A. D. Schluter, *Angew. Chem., Int. Ed.*, 2011, **50**, 737–740.
7 J. Paturej, S. S. Sheiko, S. Panyukov and M. Rubinstein, *Sci. Adv.*, 2016, **2**, e1601478.
8 J. Das, M. Yoshida, Z. M. Fresco, T.-L. Choi, J. M. J. Frechet and A. K. Chakraborty, *J. Phys. Chem. B*, 2005, **109**, 6535–6543.
9 M. Kikuchi, R. Nakano, Y. Jinbo, Y. Saito, S. Ohno, D. Togashi, K. Enomoto, A. Narumi, O. Haba and S. Kawaguchi, *Macromolecules*, 2015, **48**, 5878–5886.
10 T.-P. Lin, A. B. Chang, S.-X. Luo, H.-Y. Chen, B. Lee and R. H. Grubbs, *ACS Nano*, 2017, **11**, 11632–11641.
11 S. Morozova and T. P. Lodge, *ACS Macro Lett.*, 2017, **6**, 1274–1279.
12 A. B. Chang, T.-P. Lin, N. B. Thompson, S.-X. Luo, A. L. Liberman-Martin, H.-Y. Chen, B. Lee and R. H. Grubbs, *J. Am. Chem. Soc.*, 2017, **139**, 17683–17693.
13 X.-H. Zheng, J.-F. Zhao, T.-P. Zhao, T. Yang, X.-K. Ren, C.-Y. Liu, S. Yang and E.-Q. Chen, *Macromolecules*, 2018, **51**, 4484–4493.
14 B. Helms, J. L. Mynar, C. J. Hawker and J. M. Frechet, *J. Am. Chem. Soc.*, 2004, **126**, 15020–15021.
15 T. Kato and J. M. J. Fréchet, *Macromolecules*, 1989, **22**, 3818–3819.
16 K. B. Wagener, J. M. Boncella and J. G. Nel, *Macromolecules*, 1991, **24**, 2649–2657.
17 Y. Wei, R. Graf, J. C. Sworen, C.-Y. Cheng, C. R. Bowers, K. B. Wagener and H. W. Spiess, *Angew. Chem., Int. Ed.*, 2009, **48**, 4617–4620.
18 L. R. Middleton, S. Szewczyk, J. Azoulay, D. Murtagh, G. Rojas, K. B. Wagener, J. Cordaro and K. I. Winey, *Macromolecules*, 2015, **48**, 3713–3724.
19 H. Li, G. Rojas and K. B. Wagener, *J. Polym. Sci., Part A: Polym. Chem.*, 2018, **56**, 1705–1710.
20 M. D. Schulz and K. B. Wagener, *Macromol. Chem. Phys.*, 2014, **215**, 1936–1945.
21 L. C. da Silva, G. Rojas, M. D. Schulz and K. B. Wagener, *Prog. Polym. Sci.*, 2017, **69**, 79–107.
22 B. Inci and K. B. Wagener, *J. Am. Chem. Soc.*, 2011, **133**, 11872–11875.
23 G. Rojas, B. Inci, Y. Wei and K. B. Wagener, *J. Am. Chem. Soc.*, 2009, **131**, 17376–17386.
24 E. B. Trigg, T. W. Gaines, M. Marechal, D. E. Moed, P. Rannou, K. B. Wagener, M. J. Stevens and K. I. Winey, *Nat. Mater.*, 2018, **17**, 725–731.
25 H. Li, G. Rojas and K. B. Wagener, *ACS Macro Lett.*, 2015, **4**, 1225–1228.
26 J. Mandal, S. K. Prasad, D. S. S. Rao and S. Ramakrishnan, *J. Am. Chem. Soc.*, 2014, **136**, 2538–2545.
27 S. Chanda and S. Ramakrishnan, *Macromolecules*, 2016, **49**, 3254–3263.
28 H. Finkelmann, H. Ringsdorf and J. H. Wendorff, *Makromol. Chem.*, 1978, **179**, 273–276.
29 H. Finkelmann, M. Hap, M. Portugal and H. Ringsdorf, *Makromol. Chem.*, 1978, **179**, 2541–2544.
30 A. M. Donald, A. H. Windle and S. Hanna, *Liquid Crystalline Polymers*, Cambridge University, Cambridge, 2006.
31 S. Diele, S. Oekiner and F. Kuschel, *Makromol. Chem.*, 1987, **188**, 1993–2000.
32 C. Chovinoa, D. Guillonb and P. Gramaina, *Polymer*, 1998, **39**, 6385–6390.
33 J. A. Lv, Y. Liu, J. Wei, E. Chen, L. Qin and Y. Yu, *Nature*, 2016, **537**, 179–184.
34 R. Duran, D. Guillon, P. Gramain and A. Skoulios, *Makromol. Chem., Rapid Commun.*, 1987, **8**, 181–186.
35 S. Koltzenburg, D. Wolff, J. Springer and O. Nuyken, *J. Polym. Sci., Part A: Polym. Chem.*, 1998, **36**, 2669–2679.
36 A. A. Craig and C. T. Imrie, *J. Mater. Chem.*, 1994, **4**, 1705–1714.
37 V. P. Shibaev and N. A. Plate, *Adv. Polym. Sci.*, 1984, **60/61**, 173–252.
38 P. Davidson, *Prog. Polym. Sci.*, 1996, **21**, 893–950.
39 B. Chen, X. B. Zeng, U. Baumeister, S. Diele, G. Ungar and C. Tschierske, *Angew. Chem., Int. Ed.*, 2004, **43**, 4621–4625.
40 R. Wang and Z.-G. Wang, *Macromolecules*, 2010, **43**, 10096–10106.